Messenger RNA transfection of Dendritic cells with Mannosylated Lipopolyplexes: Impact of the surface charge on the Binding, Uptake, and mRNA expression

Christophe Delehedde[1,2], Haifei Gao[1], Ivan Ciganek[1], Cristine Gonçalves[1], Virginie Malard[1], Nathalie Rameix[2], Luc Even[2], Patrick Midoux[1], and Chantal Pichon[1]
[1]Centre de Biophysique Moléculaire, CNRS UPR4301 - Université d'Orléans, Orléans, France
[2]Sanofi R&D, Chilly-Mazarin, France

Lipopolyplexes (LPR) comprising both synthetic mRNA encoding tumour antigen, a cationic polymer and cationic liposome have proved efficacy to induce a tumour-specific immune response. Moreover, the liposome decoration with a tri-antenna of α-D mannopyranoside (Tri-Man) improves the vaccine efficiency thanks to mannose receptor mediated dendritic cells (DC) targeting. Here, we compared the binding, uptake and transfection on DC2.4 cells of cationic versus neutral Tri-Man LPR.

LPR Formation

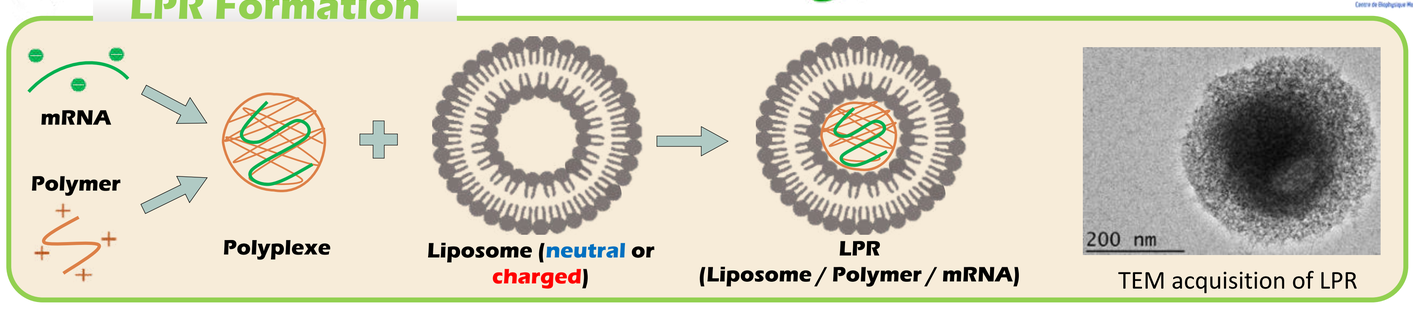

LPR composition

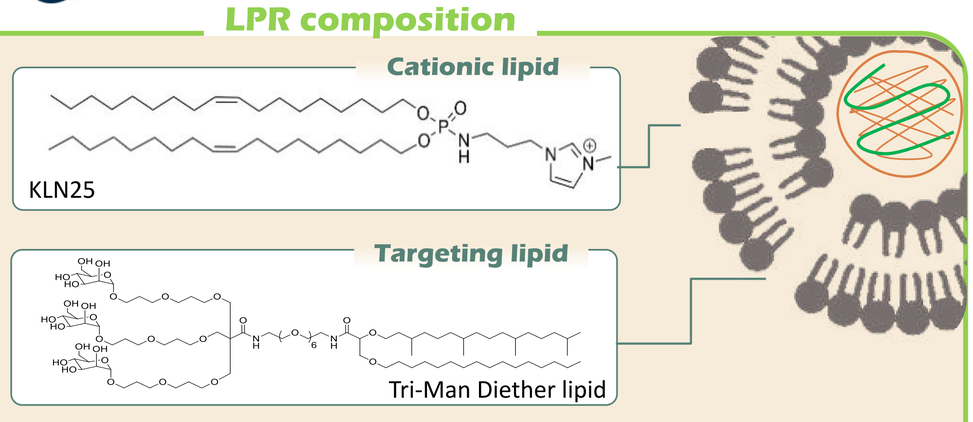

	C-Tri-ManLPR	N-Tri-man-LPR
Zeta (mV)	(+) 44.7	(+) 3.6
Size (nm)	165.2	174.3

We used liposome formulation using a targeted lipid (tri-antenna of α-D-mannopyranoside (**Tri-Man**)), a fusogenic lipid (**MM27**), and a cationic lipid (**KLN25**) or a neutral one (**DPPC**). Addition of polyplexes containing a cationic polymer and mRNA allows the formation of a lipopolyplexes (LPR) without any significant change in terms of charge and size.

Uptake experiments were carried out by flow cytometry with liposomes containing a **Fluorescein-labeled lipid**: DOPE-FITC (1,2-dioleoyl-sn-glycero-3-phosphoethanolamine).

Impact of the charge

1. Uptake study

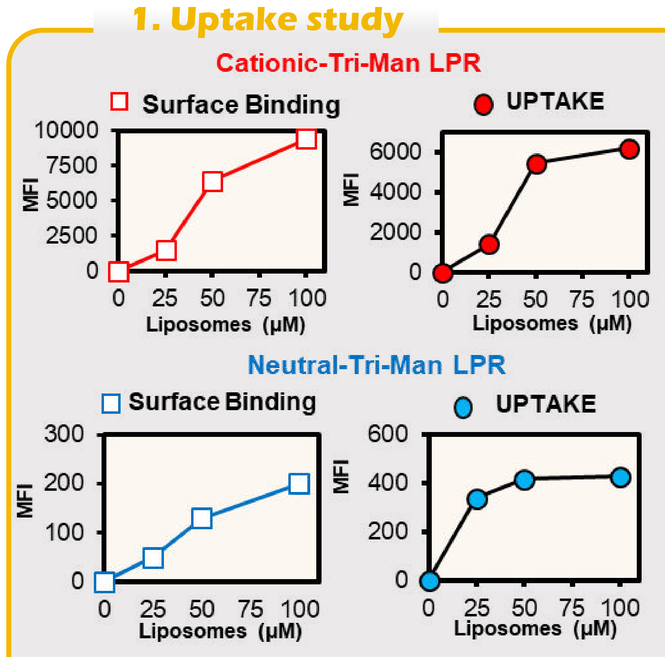

- Binding of **cationic LPR** is dramatically higher than **neutral LPR**. Positive charges conduct to nonspecific interactions **in combination** with Tri-man binding whereas there is only a specific binding through mannose receptor for neutral complexes.
- The amount of internalized **neutral LPR** is extremely low compared to that of **cationic LPR**.
- Interestingly, despite the charge of **cationic LPR,** a plateau is observed at high concentration indicating that mannose receptor targeting via Tri-Man moieties play an important role.

2. Transfection study

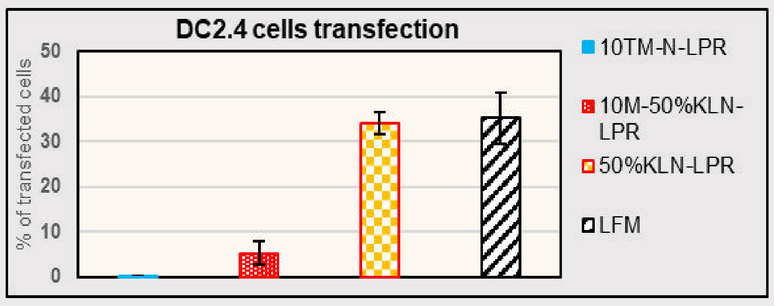

- **Neutral LPR** with 10% Tri-Man are not capable to transfect DC2.4 cell, whereas **cationic LPR** with 10% Tri-Man transfect ~5 to 10% DC 2.4 cells.
- Whilst, **cationic LPR** without Tri-Man allow up to 35% of transfection, indicating that Tri-man lipid is responsible of the low number of transfected cells with cationic formulation.

Impact of Tri-Mannosylated lipid

1. Transfection / uptake with variation of Tri-Man

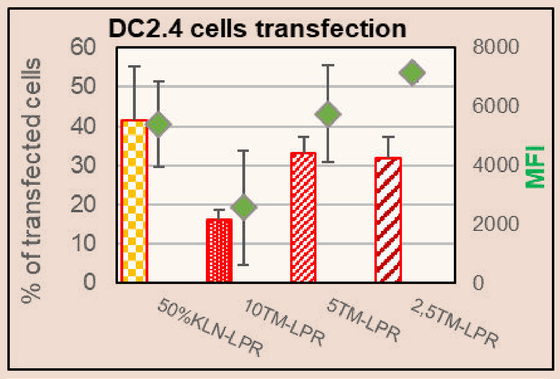

Different percentages of Tri-Man lipid were incorporated into **cationic-LPR** (2.5% / 5% / 10%TM).

Transfection data reveal that decreasing amount of Tri-Man (5% and 2.5%) tends to restore transfection efficacy. Interestingly, **MFI** associated to the transfection are also increased, but appear to be above non-Tri-Man LPR, showing a Tri-Man effect of low Tri-Man percentage bearing formulations.

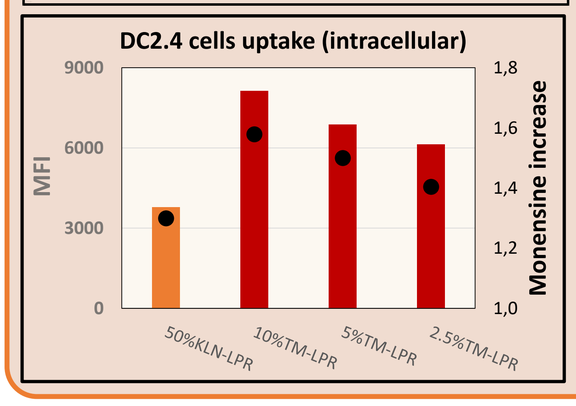

Uptake studies were conducted to assess the specificity of the different LPR. Formulations with higher percentage of Tri-Man are more taken up by the cells and routed in more acidic compartments (monensine increase ●). Decreasing the amount of Tri-Man reduces the uptake, but at 2.5% and 5%, the uptake is kept higher than non-Tri-Man LPR, showing specificity.

2. Transfection mod. *vs* non-mod. mRNA

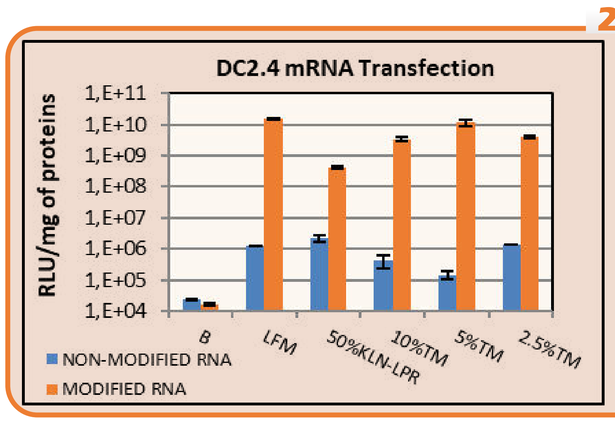

Transfection with modified mRNA shows an increase in protein translation. **Interestingly**, Tri-Man formulations have a higher improvement than non-Tri-Man formulations.

3. Biological pathway

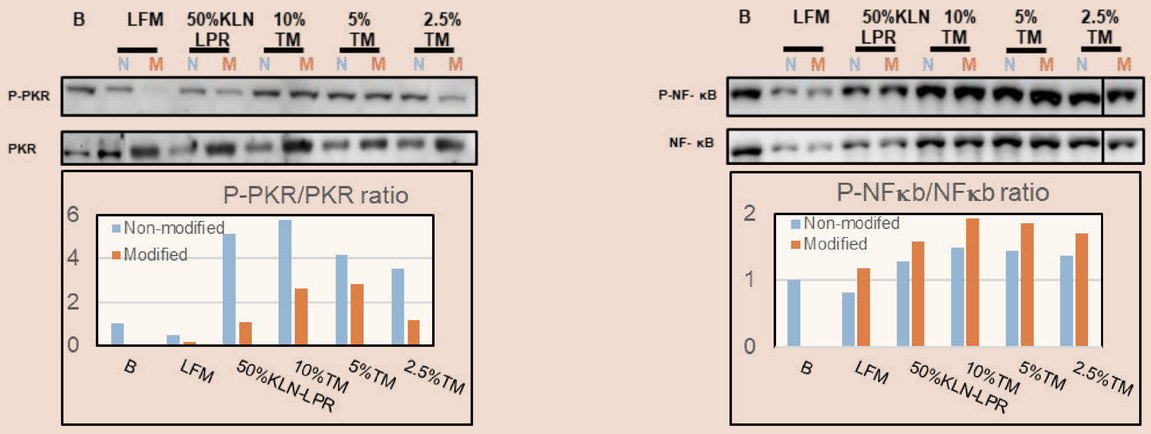

Biological pathways involved in the **regulation of translation, stress response, cytokine expression were studied** after transfection of non-modified or modified mRNA (containing CleanCap (natural cap 1 structure) and modified nucleosides (5-methoxyuridine).

Modified mRNA is used to avoid recognition by TLRs presents in late endosome (dsRNA by TLR3 and nucleosides by TLR7/8), which can lead to activation of sensors such as:

→ **PKR (RNA-dependant protein Kinase)**: After TLR sensing, activation of PKR leads to interaction with eIF2α (translation initiation factor) to stalled translation.

→ **NFκB**: Transcription factor of many genes, including those encoding pro-inflammatory cytokines & chemokines. Its activation in DCs is associated to maturation, but also to IFN-α/β production (if its activation occurs through TLRs sensing).

Transfection by Tri-Man LPRs with non-modified mRNA leads to higher PKR and NFκB activation, suggesting their accumulation in acidic compartments containing TLRs.

Use of modified mRNA decreases TLR activation and thus PKR phosphorylation, leading to efficient translation. **Interestingly**, there is a stronger activation of NFκB without any deleterious effect on transfection but likely impact DC maturation.

Conclusion

With our original Tri-Mannosylated lipid capable of targeting the mannose receptor on dendritic cell surface, we developed cationic and neutral lipopolyplexes (LPR) for mRNA delivery. Our data show that cationic Tri-Man LPR are able to keep selectivity toward DCs despite their highly positive charge.
Interestingly, large amount of Tri-Man in LPR appear to be unfavourable for mRNA transfection despite better internalization. Our results suggest that binding through mannose receptor leads to their accumulation in acidic compartments (late endosomes; lysosomes), where RNA sensing appears to be stronger. On the other hand, it has been studied that late endosomes and lysosomes are essential for mRNA transfection, thanks to mTOR signalling. Overall, our data suggest that LPR with lower amount of Tri-Man moiety made with modified mRNA could therefore be a good combination to get both a good specificity toward DCs and an efficient mRNA translation.

Synthesis of novel cyclic dinucleotides: a perspective for new STING modulators ?

Jérémy Magand,[1] Andrea Carolina Ojeda-Porras,[1] Hervé Meudal,[3] Stéphanie Rose,[2] Valérie Quesniaux,[2] Vincent Roy,[1] and Luigi A. Agrofoglio[1]

[1] ICOA, Univ. Orléans, CNRS UMR 7311, 45067 Orléans, France; [2]INEM, Univ. Orléans, CNRS UMR 7355, 45071 Orléans, France; [3]CBM, CNRS UPR4301, 45100 Orléans

Introduction

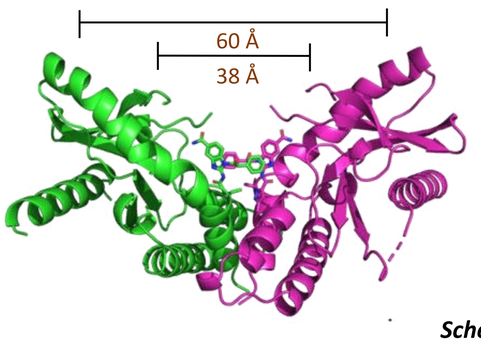

Scheme 1: *STING protein*

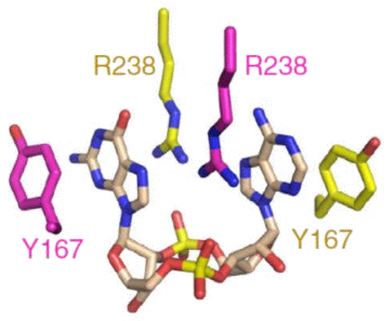

Scheme 2: *adopted conformation of 2'-3'-cGAMP into STING site*

I) STING protein is a unique and pivotal protein of cGAS-STING signaling pathway [1]; its modulation is involved in host innate immunity and STING which results to type I interferons (IFNs) and pro-inflammatory cytokines secretion that are the first mechanisms of defense to fight several infectious diseases. This protein is considered as a new attractive target to treat infections [2] and cancers [3].

II) The cyclic dinucleotide (CDN) 2',3'-GMP-AMP (cGAMP) is the endogenous agonist of STING with known antiviral activities [4] and has served as lead for new CDNs development, such as ADU-S100 [5-7]. In fact, main limitations of cGAMP are inherent to its physical properties e.g. instability regarding hydrolases and charged linkages. Neutral cGAMP analogues that feature better cellular penetrability and resistance facing hydrolysis are still needed.

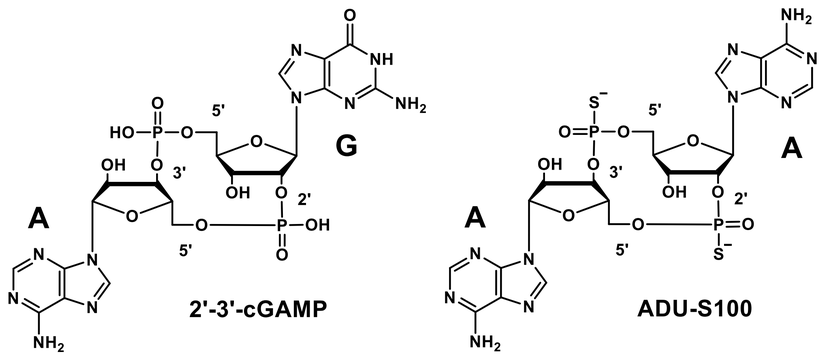

Scheme 3: *exemples of STING ligands*

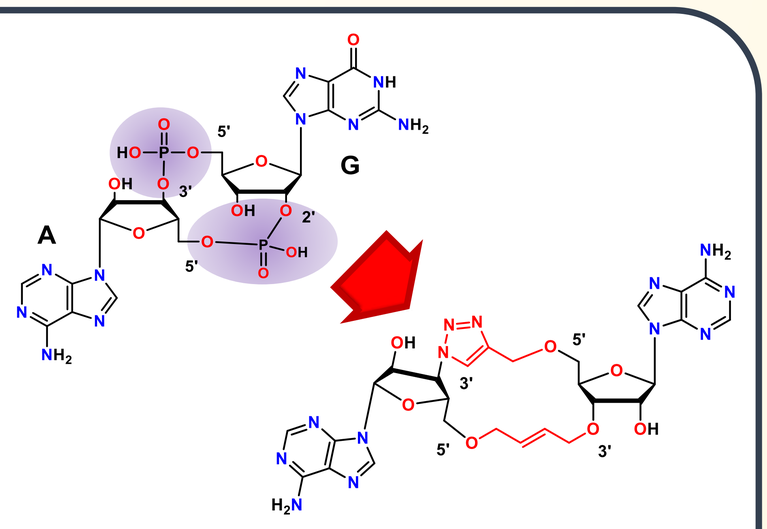

III) To overcome these issues, the designed and synthesized cGAMP analogues are bearing a triazole moiety and an unsaturated carbon chain as new 3',3'-internucleotide linkages, and having, as a dimeric CDN, the same nucleobase on each ribose moieties.

Synthesis and biological assays

3 key steps: 1,3-Huisgen cycloaddition, Ring Closing Metathesis, Vorbrüggen *N*-glycosylation

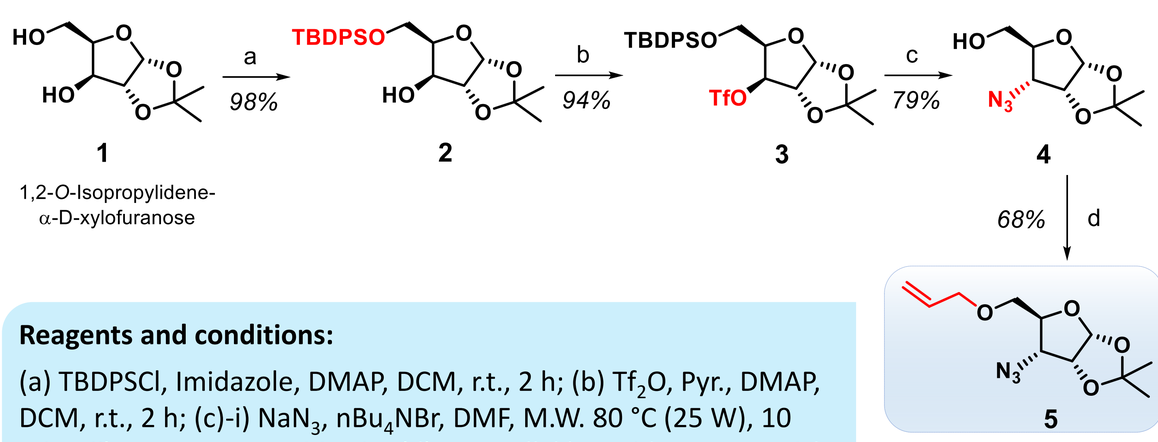

Reagents and conditions:

(a) TBDPSCl, Imidazole, DMAP, DCM, r.t., 2 h; (b) Tf_2O, Pyr., DMAP, DCM, r.t., 2 h; (c)-i) NaN_3, nBu_4NBr, DMF, M.W. 80 °C (25 W), 10 min; -ii) TBAF, THF, r.t., 30 min; (d) NaH, Allyl bromide, THF, r.t., 2 h.

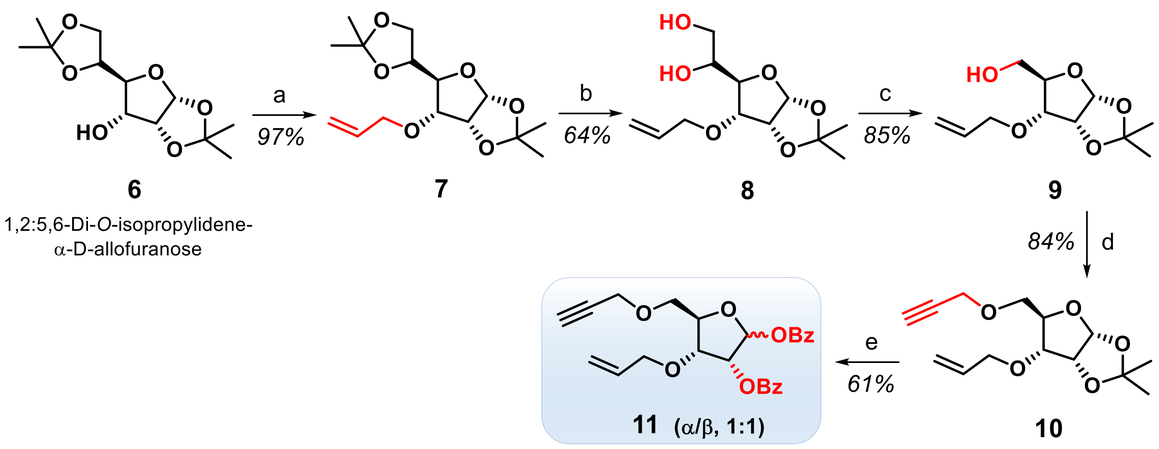

Reagents and conditions:

(a) NaH, Allyl bromide, THF, r.t., 3 h; (b) Acetic ac./Formic ac./H_2O, r.t.; (c)-i) $NaIO_4$, EtOH/H_2O, r.t., 1 h; -ii) $NaBH_4$, EtOH, r.t., 30 min; (d) NaH, Propargyl bromide, THF, r.t., 3 h;

(e)-i) Formic ac./H_2O, 60 °C, 1 h; -ii) BzCl, Pyr, DMAP, DCM, r.t., 2 h.

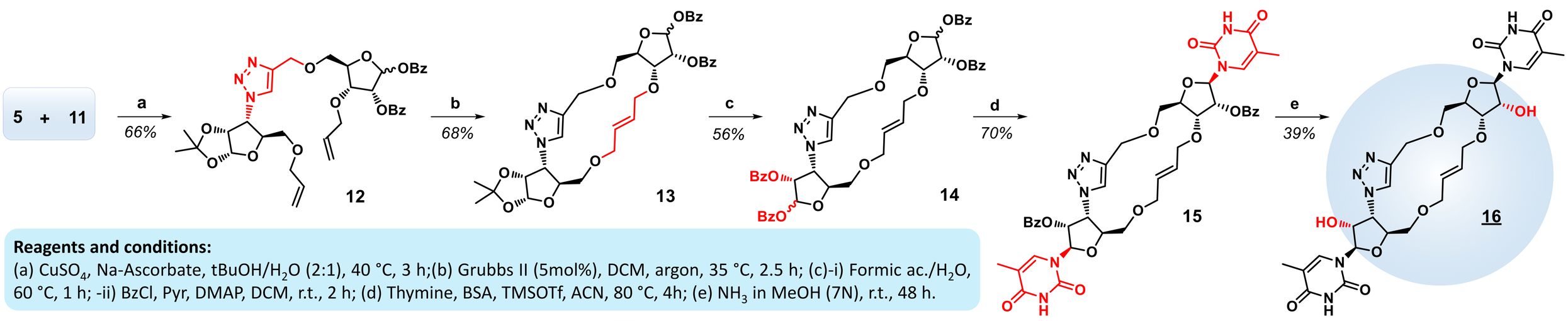

Reagents and conditions:

(a) $CuSO_4$, Na-Ascorbate, tBuOH/H_2O (2:1), 40 °C, 3 h;(b) Grubbs II (5mol%), DCM, argon, 35 °C, 2.5 h; (c)-i) Formic ac./H_2O, 60 °C, 1 h; -ii) BzCl, Pyr, DMAP, DCM, r.t., 2 h; (d) Thymine, BSA, TMSOTf, ACN, 80 °C, 4h; (e) NH_3 in MeOH (7N), r.t., 48 h.

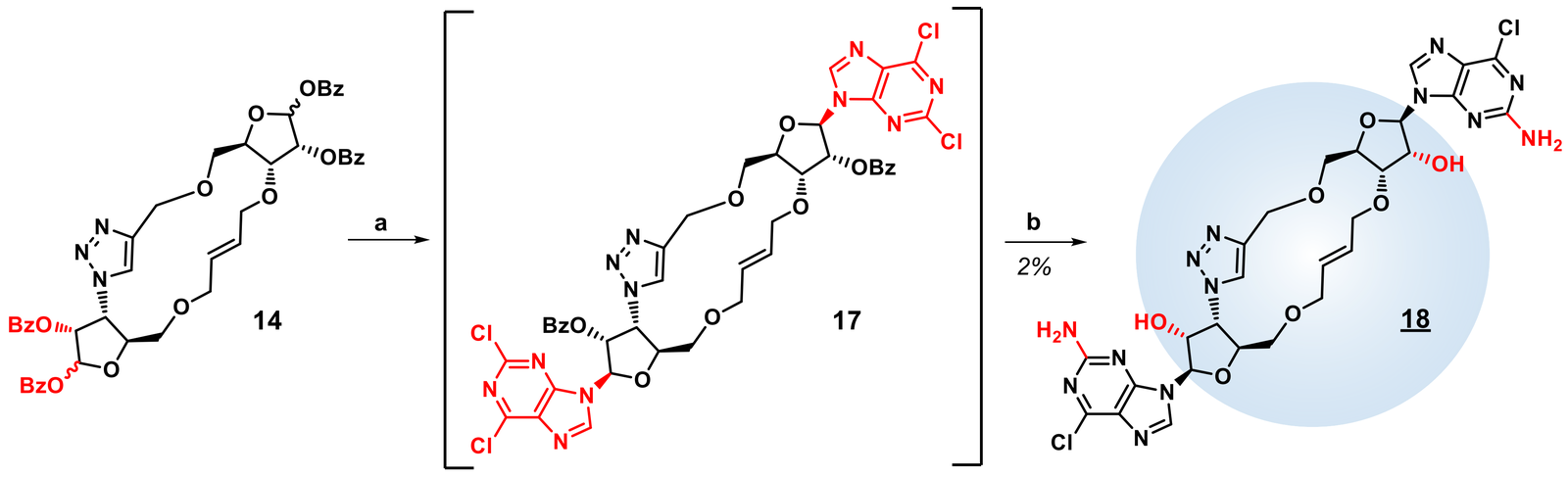

Reagents and conditions:

(a) 2,6-Dichloropurine, BSA, TMSOTf, ACN, 80 °C, 4h; (b) NH_3 in MeOH (7N), r.t., 48 h, *2%* (over two steps).

Biological and DSF assays:

-> All synthesized compounds (**16** and **18**) were evaluated to determine their activity as STING agonist or antagonist by measuring type I interferon induced secretion IP-10 in macrophages (BMDM).

-> None of them displayed a significant agonistic or antagonistic activity regarding STING.

-> **Differential Scanning Fluorimetry (DSF)** assays attested the ligands have a lower affinity with the STING protein than cGAMP .

Conclusion & Acknowlegements

Two new CDN derivatives were obtained with the previous described synthetic route. If none of them displayed a significant agonist activity, attested by DSF assays, a new set of molecules inspired from this previous work will be synthesized and tested on the protein.

Authors thanks the European Regional Development Fund (FEDER) and Region Centre Val de Loire for the financial support of EUROFERI program. J. Magand thanks MESRI and UO for PhD salary. A.C. Ojeda-Porras thanks FEDER for her salary.

References

[1] H. Ishikawa, G.N. Barber, STING is an endoplasmic reticulum adaptor that facilitates innate immune signaling, *Nature* **2008**, *455*, 674-678.

[2] G. Ni, Z. Ma, B. Damania, cGAS and STING: At the intersection of DNA and RNA virus-sensing networks, *PLoS Pathog*, **2018**, *14*, 1007148-1007154.

[3] J. Le Naour, L. Zitvogel, L. Galluzzi, E. Vacchelli, G. Kroemer, Trial watch: STING agonists in cancer therapy, *OncoImmunology* **2020**, *9*, 1777624-1777636.

[4] C. Ritchie, L. Li, cGAMP as an adjuvant in antiviral vaccines and cancer immunotherapy, *Biochemistry* **2020**, *59*, 1713-1715.

[5] Z. Wanga, Z. Xi, Chemical evolution of cyclic dinucleotides: Perspective of the analogs and their preparation, *Tetrahedron* **2021**, *87*, 132096-132124.

[6] Y. Liu, X. Lu, N. Qin, Y. Qiao, S. Xing, W. Liu, F. Feng, Z. Liu, H. Sun, STING, a promising target for small molecular immune modulator: A Review, *Eur. J. Med. Chem.* **2021**, *211*, 113113-113144.

[7] H. Zhang, Q.D. You, X.L. Xu, Targeting Stimulator of Interferon Genes (STING): A medicinal chemistry perspective, *J. Med. Chem.* **2020**, *63*, 3785-3816.

The enzymatically induced Lossen rearrangement as a bioconjugation and labelling tool

J. Tomas, M. Schuler, A. Tatibouët.
ICOA-UMR 7311, Université d'Orléans, Rue de Chartres, 45067 Orléans, France.
e-mail: josip.tomas@univ-orleans.fr

Introduction

The Myrosinase – Glucosinolate (MG) system, a naturally occurring biochemical reaction in the *Brassicales* plant order, can be used as a powerful tool to generate, *in situ*, isothiocyanates (ITCs) from stable, water soluble secondary metabolites – Glucosinolates (GLs).[a, b]

This unique enzyme-substrate system in Nature can be used as a novel bioconjugational tool for various applications such as synthesis of neoglycoproteins, selective labeling of proteins or nanoparticles functionalization.[c, d, e] To this end, different glucosinolates were designed and studied to evaluate their applications in bioconjugation.

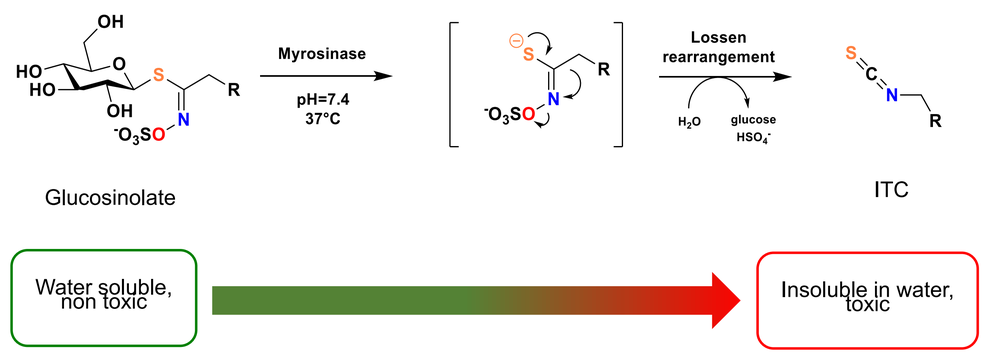

Synthesis and reactivity of azido GL

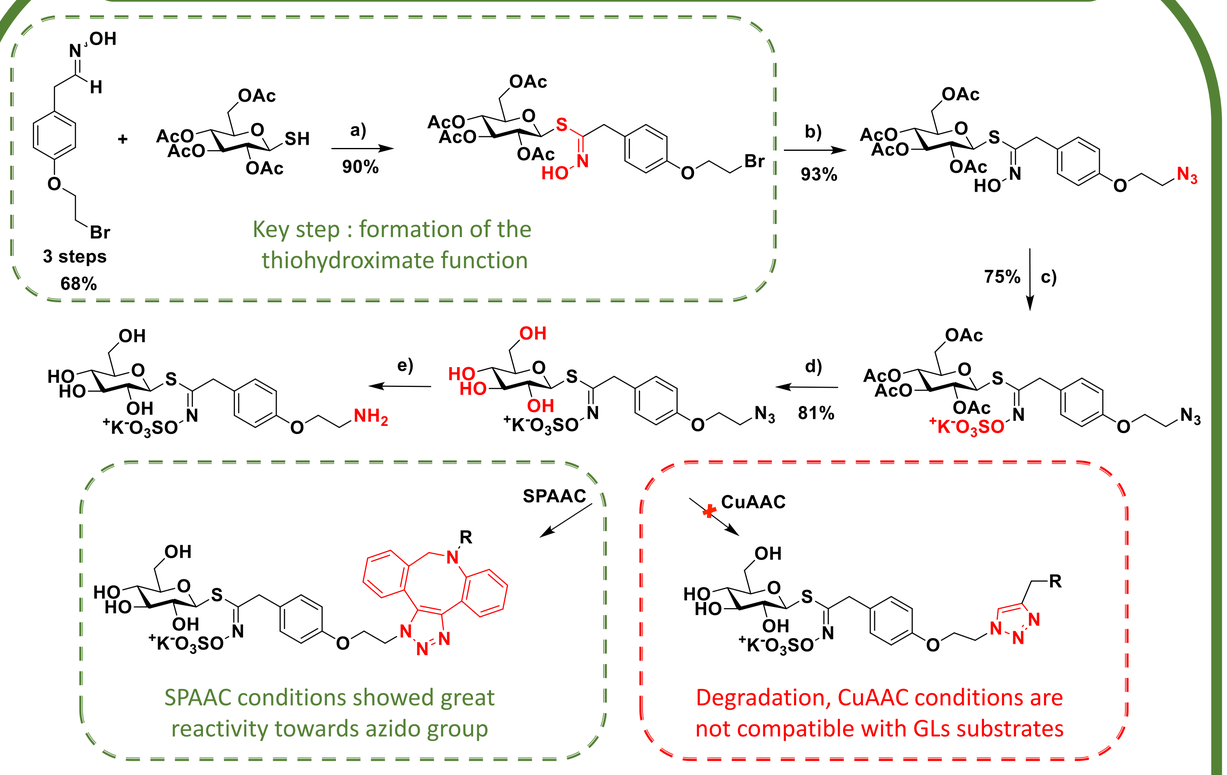

a) 1) NaOCl, DCM, rt, 30 min 2) Et_3N, rt, 2 h. b) NaN_3, DMF, 50°C, 4 h. c) $PySO_3$ complex, DMF, 50 °C, 20 h. d) MeOK, MeOH, rt, 4 h. e) PPh_3, MeOH, rt, 20 h.

These results showed that the glucosinolate moiety is not compatible with the CuAAC conditions on contrary to SPAAC ones to perform click chemistry. Nonetheless, the phosphine based reduction is perfectly compatible to generate the primary amine with quantitative yield.

Synthesis of functionalized GLs

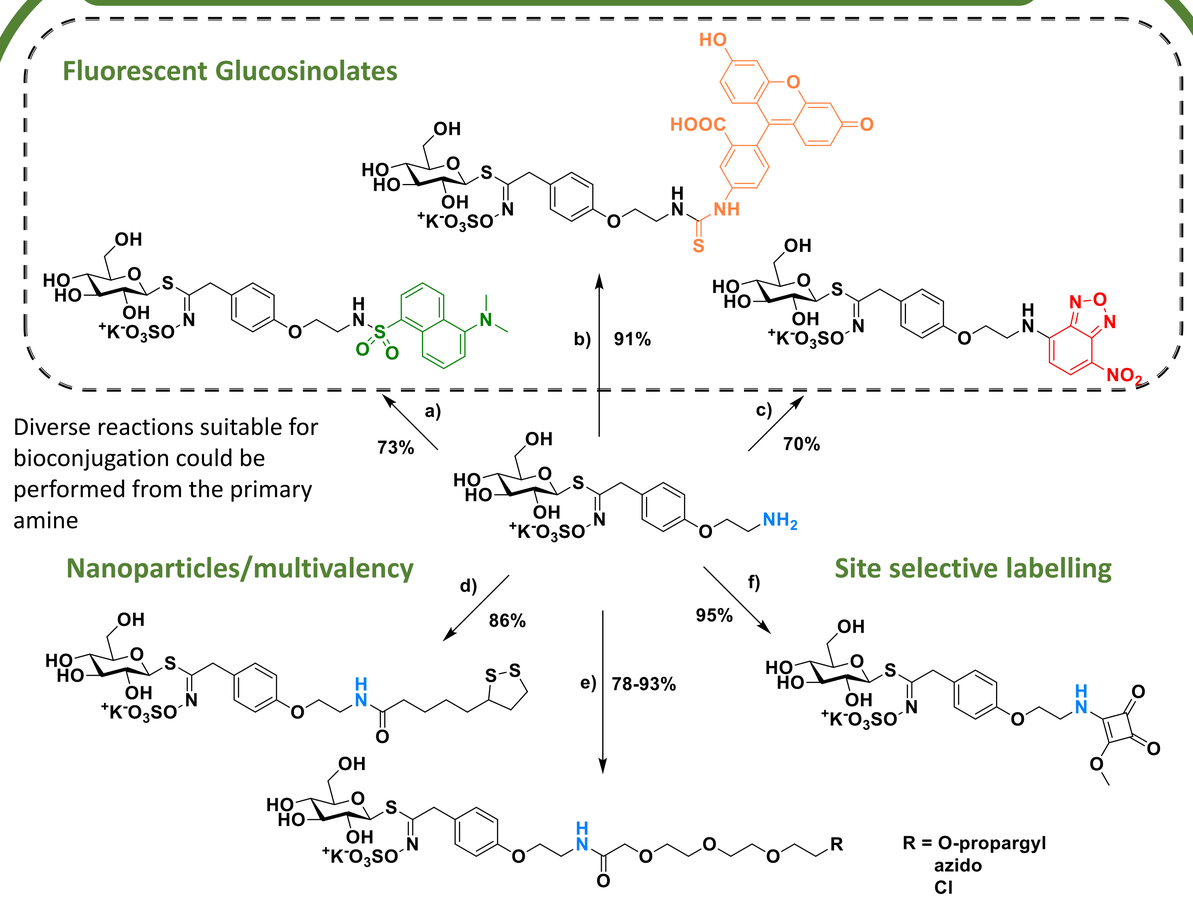

a) Dansyl chloride, Et_3N, DMF, rt, 24h. b) Fluorescein-ITC, DMF, rt, 20h. c) NBD-Cl, Et_3N, MeOH, rt, 24h. d) lipoic acid NHS ester, DMF, rt, 24h. e) NHS ester, $NaHCO_3$, H_2O, rt, 24 h. f) dimethyl squarate, MeOH, rt, 24 h

Enzymatic hydrolysis of artificial GLs

In order to use the MG-system as a bioconjugation tool, described glucosinolates need to be substrates of myrosinase.

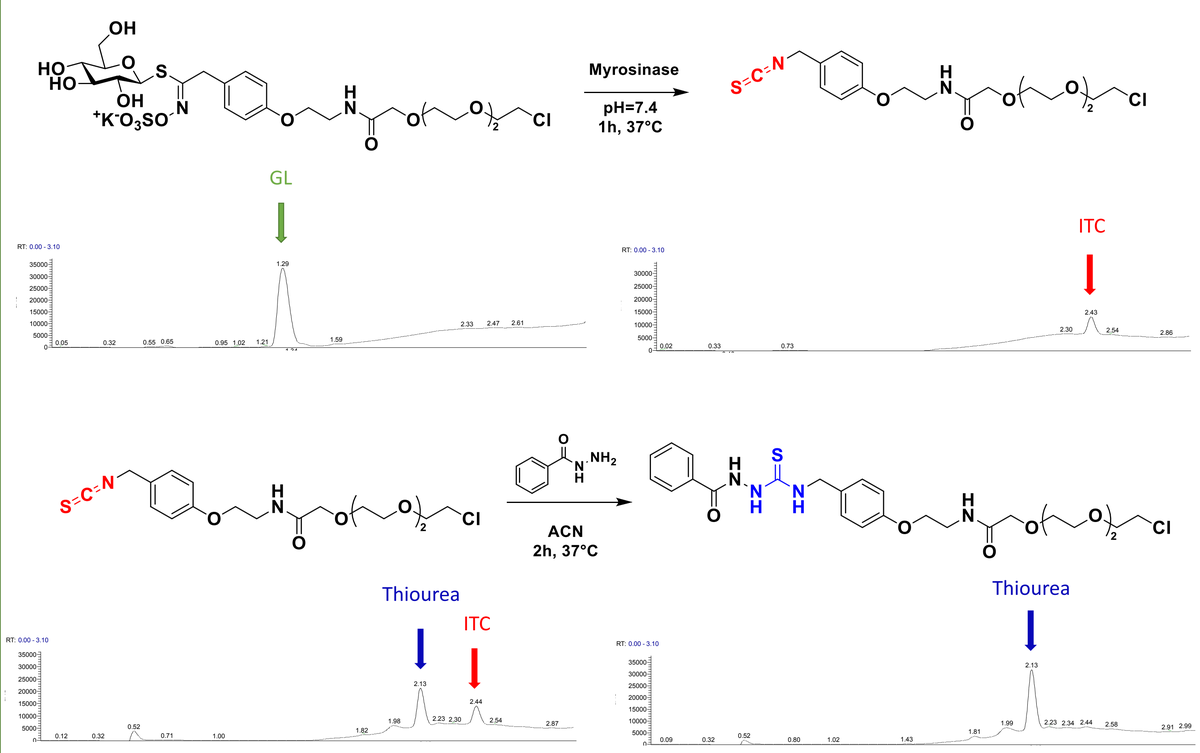

Results show that newly synthesized glucosinolates were successfully hydrolysed into ITCs, which could be trapped with a nucleophile. Hydrolysis was monitored by LC-MS using two detectors DAD and MS (not shown) (ESI, T 250 ° C)

Detecting Myrosinase activity: *p*-NP-GL

The concept and synthesis of a glucosinolate bearing a *p*-nitrophenol moiety was developed so as to be able to easily follow the myrosinase activity *in vitro.*

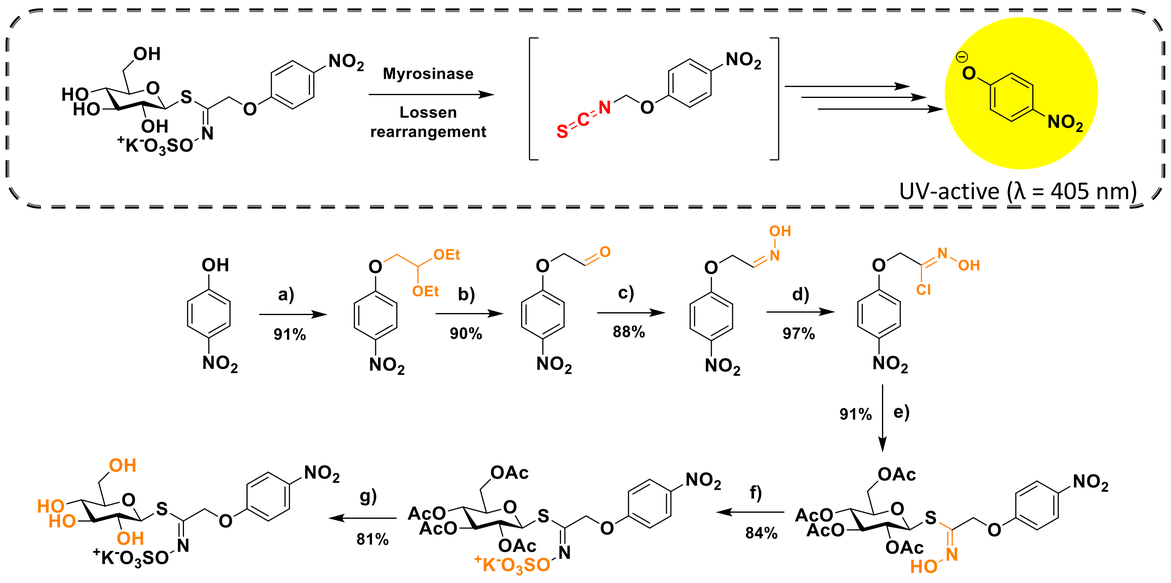

a) Bromoacetaldehyde diethylacetal, K_2CO_3, DMF, 90°C, 16h. b) TFA, H_2O, rt, 2h. c) $NH_2OH.HCl$, NaOAc, H_2O/MeOH, rt, 3h. d) NCS, DMF, rt, 2h. e) thioglucose, Et_3N, THF, 0°C to rt, 20h. f) $PySO_3$ complex, pyridine, 50°C, 20h. g) MeOK, MeOH, rt, 5h.

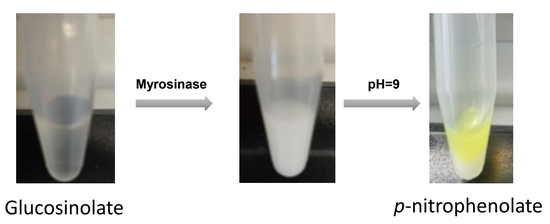

Glucosinolate hydrolysis and liberation of *p*-nitrophenolate: under basic conditions it turns yellow and is easily detected by UV.

Conclusion

In this work, we described the synthesis of glucosinolates with bioorthogonal functions and their reactivities under various conditions. We have observed that CuAAC conditions were not compatible with the glucosinolates moiety, while SPAAC conditions gave well reproducable cycloadducts together with the ability to use the easily formed primary amine to link functionalized side chains (fluorescent, lipoic, squaramide…). In addition, we demonstrate that with standard conditions, the successful hydrolysis of glucosinolates and their conversion into ITCs could easily be realized. Finally, we described an original *p*-nitrophenol Glucosinolate as a potential powerful tool to detect myrosinase activity *in vitro* opening a way to develop probes of the activities of myrosinase and myrosinase-like in complex natural media.

(a) Rollin, P.; Tatibouët, A. *C. R. Chimie*, **2011**, *14*, 194-210, b) Fahey, J. W.; Zalcmann, A. T.; Talalay, P. *Phytochemistry* **2001**, *56*, 5-51. c) Claude, B.; Cutolo, G.; Farhat, A.; Zarafu, I.; Ionita, P.; Schuler, M.; Tatibouët, A.; Morin, P.; Nehmé, R. *Analytica Chimica Acta* **2019**, *1085*, 117–125. d) Fredy, J. W.; Cutolo, G.; Poret, B.; Nehmé, R.; Hubert-Roux, M.; Gandolfo, P.; Castel, H.; Schuler, M.; Tatibouët, A.; Sabot, C.; Renard, P.-Y. *Bioconjugate Chem.* **2019**, *30* (5), 1385–1394. e) G. Cutolo, B. Didak, J. Tomas, B. Roubinet, M.Schuler, P. Lafite, R. Nehmé, L. Landemarre, A.Tatibouët *Glycobiology*, **2021**, *submitted.*

Phénomènes physico-chimiques dans le transport atmosphérique des phéromones

jami@univ-tours.fr

Ludovic Jami[1,2], Thomas Zemb[2], Jean-François Dufrêche[2], Jérôme Casas[1]

[1] Institut de Recherche sur la Biologie de l'Insecte, Université François Rabelais, 37000 Tours

[2] ICSM. Univ. Montpellier. CEA. CNRS. ENSCM. Marcoule. France.

Introduction

La communication chimique dans l'atmosphère est centrale pour de nombreux insectes et plantes mais la compréhension complète du parcours emprunté par ces molécules-signal n'est pas atteinte. Des lacunes persistent dans notre compréhension du comportement physico-chimique de ces molécules dans l'air. **Le rôle des équilibres de phase, de l'adsorption sur les surfaces ou de la réactivité des phéromones dans l'atmosphère est encore peu connu. [1, 3]**

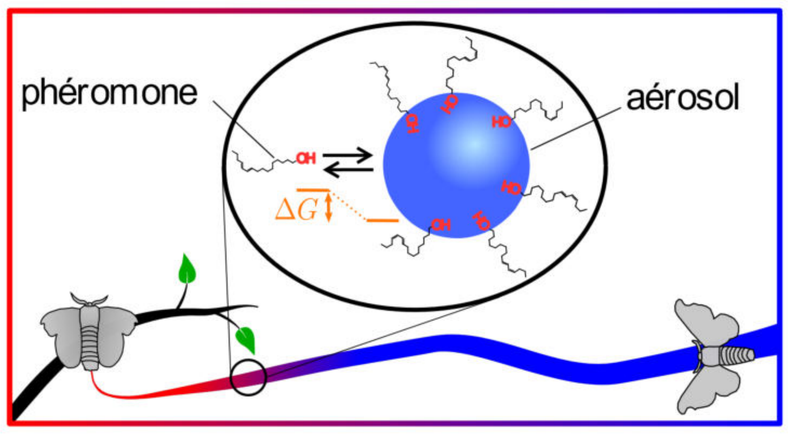

Figure 1

Nous nous intéresserons ici en particulier à l'**adsorption des phéromones sur les aérosols**, les phéromones pouvant ainsi être transportées sur de longues distances de manière groupée (fig. 1). La **modélisation de ces mécanismes, de l'échelle moléculaire à celle de la communication chimique**, nous permet de quantifier l'importance de ces effets pour la communication phéromonale dans les écosystèmes.

Modèle macroscopique du transport des phéromones sur les aérosols [1]

Temps de sorption (s) en fonction du rayon des aérosols (µm)

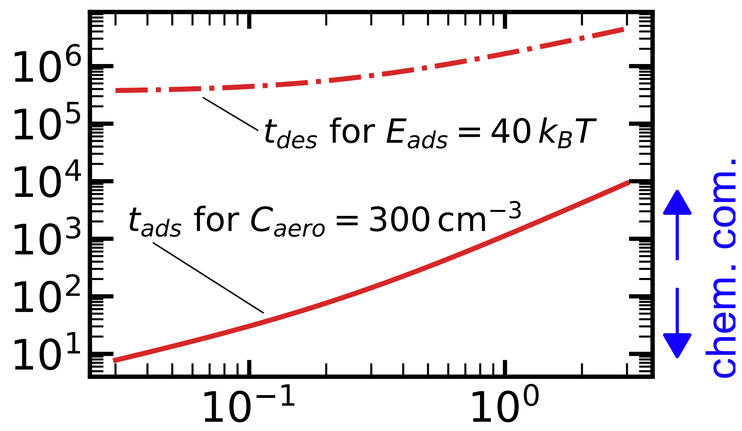

Figure 2

- ✓ Modèle de Hertz et diffusion limitante pour la **cinétique d'adsorption** des phéromones sur les aérosols
- ➢ **L'adsorption est un processus rapide** qui a lieu pendant la communication phéromonale (fig. 2)
- ✓ Modèle de **réaction-diffusion** pour la dynamique couplée du transport et de l'adsorption des phéromones
- ➢ Les phéromones sont transportées par les aérosols si l'enthalpie libre d'adsorption $\Delta_r G > 22\ k_B T$ (fig. 3)

Nombre de phéromones par aérosol

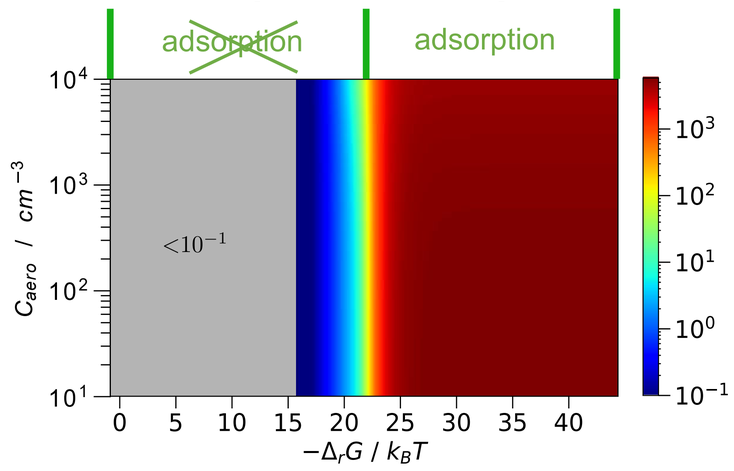

Figure 3

Simulations moléculaires pour la thermodynamique de l'adsorption [2]

- ✓ L'enthalpie libre, l'enthalpie $\Delta_r H$ et l'entropie $\Delta_r S$ d'**adsorption d'une phéromone individuelle sur une surface aqueuse** sont évaluées par simulation libre et biaisée (fig. 4)
- ➢ L'adsorption est dans ce cas trop faible pour que les phéromones de *B. mori* soient transportés par les aérosols (table)

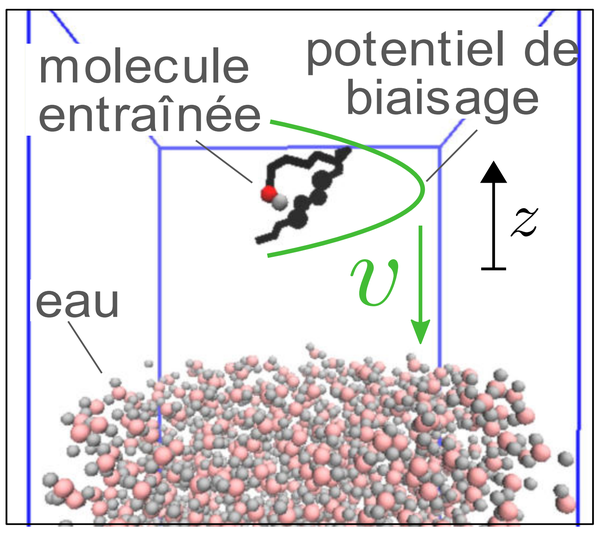

Figure 4

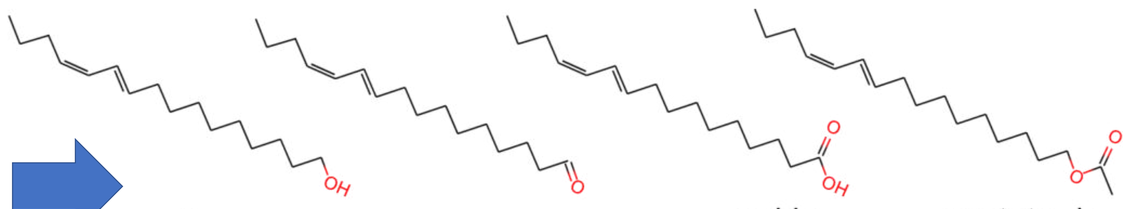

	bomby kol	bomby kal	acide bomby koique	acetate de bomby ky le
$\Delta_r G / k_B T$	-9.17	-5.49	-10.45	-7.73
$\Delta_r H / k_B T$	-38.34	-30.29	-47.35	-41.73
$\Delta_r S / k_B$	-29.17	-24.80	-36.90	-34.00

Table

Perspectives

- ❖ Adsorption collective des phéromones
- ❖ Aérosols non aqueux
- ❖ Transport atmosphérique turbulent [4]

Impacts

- ❖ Contrôle durable d'insectes nuisibles par émission de phéromones
- ❖ Effet de la pollution sur les écosystèmes
- ❖ Olfaction et écologie-chimique

Références

[1] Jami, L., Zemb, T., Casas, J., & Dufrêche, J. F. (2020). How Adsorption of Pheromones on Aerosols Controls Their Transport . ACS central science, 6(9), 1628-1638

[2] Jami, L., Zemb, T., Casas, J., & Dufrêche, J. F. (2021). In prep.

[3] Ren, Y., McGillen, M. R., Daële, V., Casas, J., & Mellouki, A. (2020). The fate of methyl salicylate in the environment and its role as signal in multitrophic interactions. Science of the Total Environment, 749, 141406.

[4] Celani, A., Villermaux, E., & Vergassola, M. (2014). Odor landscapes in turbulent environments. Physical Review X, 4(4), 041015.

Remerciements

- Projet PHEROAERO de la region Centre
- ANR MULTISEPAR 18-CE29-0010
- Aide à la mobilité école doctorale SSBV

Biotechnocentre – 7,8 octobre 2021 - Center Parc - Les Hauts de Bruyères

Target-mediated pharmacokinetics of cetuximab: target occupancy influences progression-free survival

Sarah LOBET[1*], Gilles PAINTAUD[2,3], Nicolas AZZOPARDI[4], Christophe PASSOT[5], Morgane CAULET[6], Romain CHAUTARD[1,6], Celine VIGNAULT-DESVIGNES[2,3], Olivier CAPITAIN[5], David TOUGERON[7], Michelle BOISDRON-CELLE[5], David TERNANT[2,3] , Thierry LECOMTE[1,6]

[1]Inserm UMR 1069, Nutrition Croissance et Cancer, Tours University, France; [2]EA4245 Transplantation, Immunologie, Inflammation, Tours University, France; [3]Pharmacology Department, Tours University Hospital, France; [4]EA7501 GICC, Team PATCH, Tours University, France; [5]Oncopharmacology-Pharmacogenetics Department INSERM U892, Institut de Cancérologie de l'Ouest site Paul Papin, Angers, France; [6]Gastroenterology and Digestive oncology Department, Tours University Hospital, Tours, France; [7]Gastroenterology Department, Poitiers University Hospital, France.

INTRODUCTION

Cetuximab (CTX) is an anti-EGFR monoclonal antibody (mAb) approved in the treatment of metastatic colorectal cancer (mCRC). CTX binds to its target with large affinity, leading to the formation of CTX-EGFR complexes that are cleared by several mechanisms. The increase in target-mediated elimination is due to a high target turnover and/or a fast elimination of complexes, leading to **nonlinear elimination.** The joint kinetics of mAb and target kinetics are usually described using **target-mediated drug disposition (TMDD) models** (1).

Relationship between CTX exposure and efficacy has not been clearly established due to several confounding factors. An increased global clearance was shown to be associated with shorter progression-free survival (PFS) (2). This suggests that shorter survival is associated with larger CTX consumption, and therefore higher target amounts.

Objectives: to develop a TMDD model allowing the description of EGFR kinetics following CTX treatment and to investigate the association between target occupancy and patients survival.

MATERIALS & METHODS

Data :

- Multicenter phase II study (*ClinicalTrials.gov identifier: NCT00559741*) in patients with mCRC *(n=91)*
- CTX administration: loading dose of 400mg/m² followed by 250mg/m² weekly doses

PK analysis :

- Concentration of CTX in blood sample *(n=1296)*→ ELISA technique
- Population approach (3) and a 2-compartments quasi-steady-state (QSS) TMDD model (4) (fig.1)

Survival analysis :

- Investigation of various target occupancy metrics on PFS
- Cox proportional-hazards models (5)

Model-based simulations (6) :

- Simulations of 90% prediction intervals of CTX and free EGFR concentrations over time (n=1000)
- Dosing regimens investigated : 250mg/m² QW, 500mg/m² Q2W and 750mg/m² Q3W

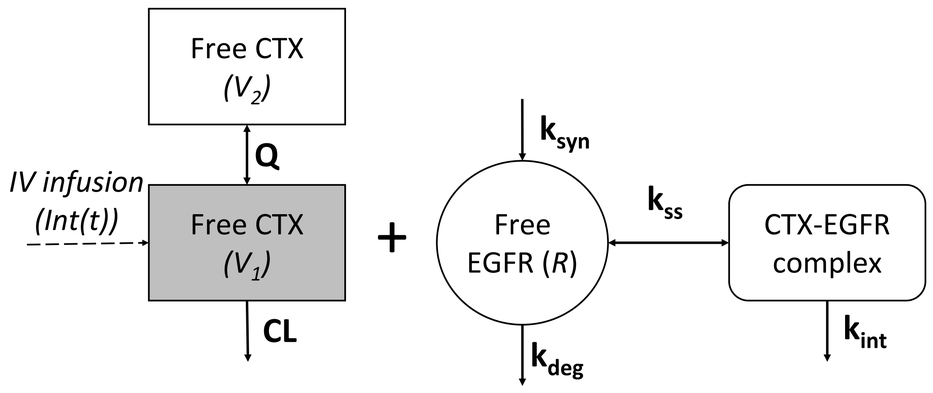

Figure 1 : Structure of a two-compartments QSS TMDD model for CTX and EGFR interaction in mCRC patients.

In(t) is the infusion rate; V_1 and V_2 are the volume of the central and peripheral compartments ; CL and Q are the global and intercompartmental clearance constant of CTX, K_{SS}, steady-state rate constant; k_{syn} and k_{deg}, the EGFR synthesis and degradation rate constant; k_{int}, the complex internalisation rate constant. In grey is represented the measured concentration of the system.

RESULTS

PK analysis:

- CTX concentration-time data were satisfactorily described by the TMDD model.
- All TMDD parameters were estimated with good accuracy (table 1).

Table 1 : Population PK parameter estimates

Parameters	Estimates	RSE (%)
Fixed effects		
V_1 (L)	2,7	3,5
β_{V_logBSA}	1,11	26,9
CL (L.day^{-1})	0,37	5,9
β_{CL_SEXE}	0,22	32,0
β_{CL_logALB}	-0,94	31,6
V_2 (L)	4,6	6,5
Q (L.day^{-1})	1,0	0,84
R_0 (nM)	2,4	10,7
k_{int} (day^{-1})	4,5	21,8
k_{deg} (day^{-1})	15,1	7,4
K_{SS} (nM)	0,61	17,4
Random effects		
ω_{V1}	0,28	10,5
ω_{CL}	0,28	9,9
ω_{V2}	0,48	12,3
ω_{R0}	0,29	19,9
Error model parameters		
σ_{prop}	0,23	2,4

RSE: relative standard errors; R_0 is the baseline of EGFR; β: scaling factor for the influence of that covariate; ω: between subject variability parameter; σ_{prop}: proportionnal parameter

Survival analysis:

- Among target occupancy metrics tested, R_{42days} was the one which presented the highest association with PFS. Higher R_{42days} was found to be associated with poorer survival (fig. 2).

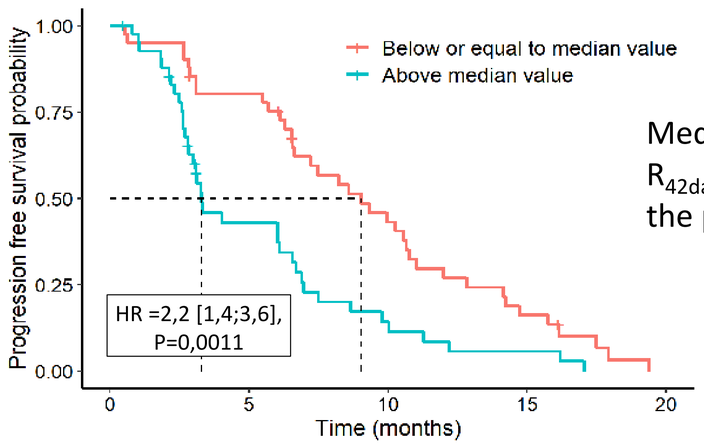

Median PFS was 9.0 months for patients with R_{42days}≤0.014nM (median value estimated in the population) and 3.3 months for others.

Figure 2 : Kaplan-Meier curves of PFS according R_{42days}

Model-based simulations:

- Simulations of CTX and free EGFR concentrations over time (fig. 3)

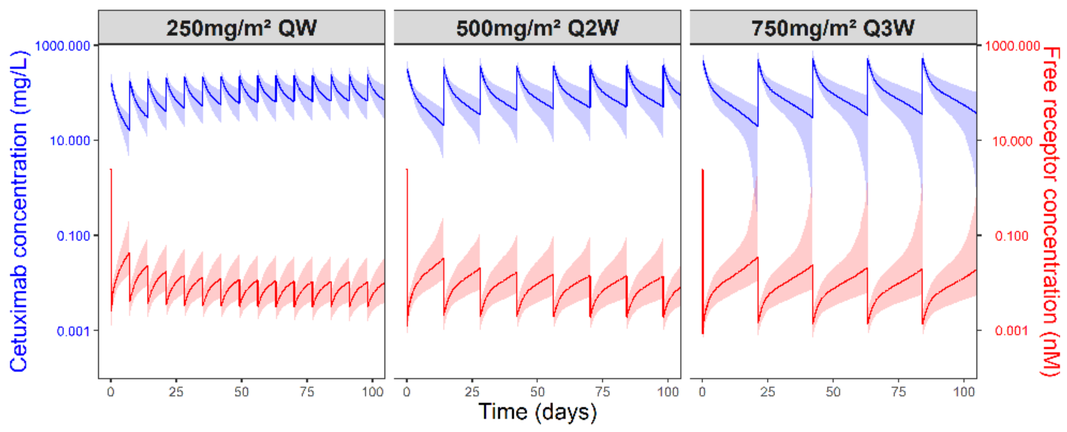

Figure 3 : Model-based simulation of CTX and free EGFR concentrations

On the top, the median PK profile of the population (blue line) and 90 % prediction interval (blue surface); the median R over the time of the population (red line) and 90 % prediction interval (red surface).

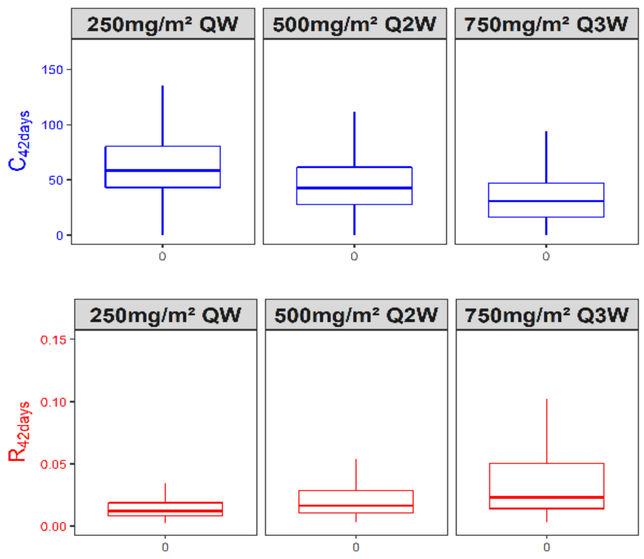

Figure 4 : Distribution of C_{42days} and R_{42days}

On the top, the distribution of C_{42days} (blue boxplot) and on the bottom the distribution of R_{42days} (red boxplot)

CONCLUSIONS

- First study describing TMPK of cetuximab using a QSS TMDD model.
- Quantification of the EGFR kinetics, which influences PFS.
- **500mg/m² Q2W regimen could be used instead of 250mg/m² QW in almost patients.**

CONTACT : sarah.lobet@etu.univ-tours.fr

REFERENCES

(1) Mager DE, Jusko WJ. *J Pharmacokinet Pharmacodyn*. 2001; (2) Azzopardi N, et al. *Clin Cancer Res*. 2011; (3) Monolix version 2020R1. *Antony, France: Lixoft SAS*. 2020; (4) Gibiansky L, et al. *J Pharmacokinet Pharmacodyn*. 2008; (5) Therneau T. *R package « survival » version 3.2-7*. 2020; (6) Simulx version 2020R1. *Antony, France: Lixoft SAS*. 2020.